Backscattering enhancement for Marshall-Palmer distributed rains for a W-band nadir-pointing radar with a finite beam width

Satoru Kobayashi, Simone Tanelli, Eastwood Im
Jet Propulsion Laboratory,
California Institute of Technology
4800 Oak Grove Dr. MS. 300-243 Pasadena, CA, 91109, USA
E-mail: satoru@radar-sci.jpl.nasa.gov

Tomohiro Oguchi
Kanto Gakuin University
1-50-1 Mutsu'ura Higashi
Kanazawa, Yokohama, 236-8501, Japan

***Abstract*— A finite beam theory of the multiple scattering associated with backscattering enhancement was derived in a previous study by the authors for a layer of spherical raindrops. Although the previous theory clarified the reflectivity of multiple scattering for a finite beam width, it can be applied only to a distribution of spherical raindrops of uniform size. In this paper, we expand the previous theory to be applied to a generic drop size distribution with spheroidal raindrops including spherical rain drops. In this paper, we expand the previous theory to be applied to a generic drop size distribution with spheroidal raindrops including spherical raindrops. Results will be used to discuss the multiple scattering effects on the backscatter measurements acquired by a W-band (95-GHz) nadir-pointing radar. Our findings will have direct applications to spaceborne cloud radar remote sensing, including NASA's CloudSat Mission, which is scheduled for launch in the summer of 2005. In general, change of raindrop shape from sphere to spheroid brings about spatial anisotropy not only in the scattering matrix but also in the propagation wave constants. This spatial anisotropy causes no effect on the first order scattering at nadir, while its effect on second order scattering must be carefully treated. For nadir operation, it has been demonstrated that the change in the spatial anisotropy brought by the non-spherical water particles gives negligible difference from our spherical particle approximation for the second order copolarized reflectivity, while for the cross polarized intensity, a small difference of less than 10 % appears. As an illustration, for nadir operation of a 95 GHz radar, both the sphere and spheroid approximations give the total increment in copolarized reflectivity of 1 dB for 10 mm/hr rain of a layer thickness of 100 m along with the Marshall-Palmer distribution. This increment must be subtracted from measured copolarized intensity in order to retrieve the correct amount of precipitation. Since our primary concern is to correct the total copolarized reflectivity, this result seems to legitimate to use spherical particles for estimating the effect of multiple scattering as a first approximation.**

I. Introduction

Millimeter-wavelength weather radars have been extensively used to increase accuracy of measuring hydrometeor number densities (e.g. raindrops, liquid-cloud particles). In this frequency regime, multiple scattering effects become important so as to be taken into account when using radar reflective intensity in retrieval algorithms of hydrometeor density. The occurrence of multiple scatterings was confirmed in 35 GHz radar measurements by the presence of depolarized signals reflected from spherical rain drops [1], [2].

From the early 1970's to the early 1990's, multiple scattering in randomly distributed particles was intensively studied through the analytical method of electromagnetic wave [3], [4], [5], [6], [7]. In the course of study, two main contributions of multiple scattering to reflective intensity were revealed; one is the conventional multiple scattering called ladder term, and the other called cross term, is contribution from interference of two ray paths mutually satisfying the condition of time-reversal paths. For monostatic radars, the cross term becomes comparable to the ladder term, resulting in backscattering enhancement.

In all the previous theoretical works, a plane wave is injected to a layer of randomly distributed particles, and the reflected wave is collected by a receiver at infinite range. On the other hand, in remote sensing, a spherical wave with a finite beam width, usually approximated as a Gaussian antenna pattern within the antenna mainlobe, is injected, and the reflected wave is received by an antenna at a finite range. Kobayashi et al. [8], [9] recently derived a finite beam theory of the multiple scattering associated with backscattering enhancement. The theory clarified that for a radar footprint smaller than the mean free path, the backscattering-enhancement reflectivity corresponding to spherical waves is significantly less pronounced than in the case of the plane wave theory. However the above theory can be applied only to a distribution of spherical raindrops of uniform size. In this paper, we expand the previous theory to be applied to a generic dropsize distribution with spheroidal raindrops including spherical rain drops. When ice-particles are approximated as spheroids as described in [10], the derived theory can be applied to ice-particle clouds that have large albedos, to calculate the effect of multiple scattering. This application is important for CloudSat mission, and will be reported in the future.

II. Formalism

In general, change of raindrop shape from sphere to spheroid brings about spatial anisotropy not only in the scat-

tering matrix but also in the propagation wave constants. Thus the propagation Green functions in [8], [9] must be changed to dyadic forms. Suppose that spheroidal particles are aligned in a preferential direction, defined by polar angles θ_b and φ_b. Since the principal axes of wave propagations coincide with two directions $\widehat{\Theta}$ and $\widehat{\Phi}$ in the body frame of the spheroids, the propagation dyadic Green function is represented in the diagonal form

$$\overline{G}_{11}(\mathbf{r},\,\mathbf{r}') \approx (4\pi)^{-1}\,|\mathbf{r}-\mathbf{r}'|^{-1}\,|\beta\rangle\;exp[ik_\beta\,|\mathbf{r}-\mathbf{r}'|]\,\langle\beta\,| \tag{1}$$

in which the Dirac notation has been used. Namely the dummy vector-component β represents one of $\widehat{\Theta}$ and $\widehat{\Phi}$, and β is summed up over $\widehat{\Theta}$ and $\widehat{\Phi}$. The complex wave number k_β that is a function of the polar coordinate Θ is given by the Foldy approximation [11]:

$$k_\beta(\Theta) = k + 2\pi k^{-1}\int da\,N(a)F_{\beta\beta}(\hat{r},\,\hat{r};a) \tag{2}$$

where k is the wavenumber in air, and the unit vector $\hat{r}$ represents the direction specified by the polar coordinate Θ and Φ. $N(a)$ is a drop size distribution function, and $F_{\beta\beta}(\hat{r},\,\hat{r};a)$ denotes the $\beta\beta$ component of the forward scattering amplitude matrix for an diameter 'a'. Note that k_β depends only on Θ in the body frame of spheroids due to its axial symmetry. In the same manner, the incident wave $\boldsymbol{\psi}(\mathbf{r}')$, and the dyadic Green function of the received wave $\bar{G}_{01}(\mathbf{r},\,\mathbf{r}')$ can be rewritten

$$\begin{aligned}\boldsymbol{\psi}(\mathbf{r}') &\approx \sqrt{P_t\,G_0\,/4\pi}\,r_s^{-1}exp[ikr_s]\,exp[-r_\perp^{'2}/4\sigma_r^2]\\ &\quad |\beta_2\rangle\;exp[i\mathbf{K}_{i\beta_2}\mathbf{r}']\,\langle\beta_2\,|\,\boldsymbol{\psi_0}\rangle\end{aligned} \tag{3}$$

$$\begin{aligned}\bar{G}_{01}(\mathbf{r},\,\mathbf{r}') &\approx \sqrt{\pi\,G_0\,/k^2}\,r_s^{-1}exp[ikr_s]\,exp[-r_\perp^{'2}/4\sigma_r^2]\\ &\quad |\beta_1\rangle\;exp[i\mathbf{K}_{s\beta_1}\mathbf{r}']\,\langle\beta_1\,|\end{aligned} \tag{4}$$

$$\sigma_r^2 = r_s^2\,\theta_d^2/2^3 ln2 \tag{5}$$

in which a large range $r_s \gg |\mathbf{r}'|$ and a small 3-dB aperture angle $\theta_d \ll 1$ have been assumed. $r'_\perp$ denotes the transverse length of the point $\mathbf{r}'$ that is orthogonal to the layer thickness of d as shown in Fig. 1. P_t and G_0 denote the transmitting power and the center gain of an antenna respectively. $\boldsymbol{\psi_0}$ represents the unit vector of an initial polarization. The dummy vector-components β_1 and β_2 represent taking sums over $\widehat{\Theta}$ and $\widehat{\Phi}$. The foot print radius σ_r is defined in Eq. 5. The complex wave numbers in the incident and received directions are defined respectively in the forms of

$$\mathbf{K}_{i\beta_2} \approx Re(k_{i\beta_2})\hat{k}_i - i\kappa"_{zi\beta_2}\hat{z} \tag{6}$$

$$\mathbf{K}_{s\beta_1} \approx Re(k_{s\beta_1})\hat{k}_s + i\kappa"_{zs\beta_1}\hat{z} \tag{7}$$

in which the imaginary parts are defined with the incident (θ_{inc}) and received (θ_s) angles as

$$\kappa"_{zi\beta_2} = -Im(k_{i\beta_2})/cos\theta_{inc} \tag{8}$$

$$\kappa"_{zs\beta_1} = Im(k_{s\beta_1})/cos\theta_s \tag{9}$$

In Eqs. 6- 9, the complex wave numbers in the incident and received directions, denoted by $k_{i\beta_2}$ and $k_{s\beta_1}$ respectively, can be defined in the same manner as Eq. 2. For later use, the real and imaginary parts of the z-components of Eqs. 6 and 7 are rewritten along with Eqs. 6-9 to the forms

$$K_{zi\alpha} = -k'_{zi\alpha} - i\kappa"_{zi\alpha} \tag{10}$$

$$K_{zs\alpha} = k'_{zs\alpha} + i\kappa"_{zs\alpha} \tag{11}$$

Using Eqs. 1-11 in the same manner as Kobayashi et al. [8], [9], the received signals of the first order scattering (the first order ladder term) can be represented for nearly backscattering condition:

$$\begin{aligned}I_L^{(1)} &= B\cdot Re\,[\,\{1-e^{-i(K^*_{zs\alpha_1}-K_{zs\beta_1}+K_{zi\beta_2}-K^*_{zi\alpha_2})d}\}\\ &\quad \{i(K^*_{zs\alpha_1}-K_{zs\beta_1}+K_{zi\beta_2}-K^*_{zi\alpha_2})\}^{-1}\int da\,N(a)\\ &\quad \left\{\langle u\,|\,\alpha_1\rangle\left\langle\alpha_1\left|F(\hat{k}_s,\,\hat{k}_i;a)\right|\alpha_2\right\rangle\langle\alpha_2\,|\,\boldsymbol{\psi_0}\rangle\right\}^*\\ &\quad \left\{\langle u\,|\,\beta_1\rangle\left\langle\beta_1\left|F(\hat{k}_s,\,\hat{k}_i;a)\right|\beta_2\right\rangle\langle\beta_2\,|\,\boldsymbol{\psi_0}\rangle\right\}\,]\end{aligned} \tag{12}$$

with a constant

$$B = P_t G_0^2\lambda^2\theta_d^2\,(2^9\pi^2\,ln2\,r_s^2)^{-1} \tag{13}$$

In Eq. 12, u represents one of unit vectors of the received orthogonal polarization, e.g. h and v. Since u is treated as dummy vector in Eq. 12, we must take sum over h and v.

The second order ladder term can be represented:

$$\begin{aligned}I_L^{(2)} &= B\int da_1N(a_1)\int da_2N(a_2)\,\{\int_0^\infty d\eta\frac{\eta}{1+\eta^2}\\ &\quad \int_0^{2\pi}d\varphi\,Re\,[\,\left\{\langle u\,|\,\alpha_1\rangle\left\langle\alpha_1\left|F(\hat{k}_s,\,\hat{r};a_2)\right|\gamma\right\rangle\right.\\ &\quad \left\langle\gamma\left|F(\hat{r},\,\hat{k}_i;a_1)\right|\alpha_2\right\rangle\langle\alpha_2\,|\,\boldsymbol{\psi_0}\rangle\,\}^*\\ &\quad \left\{\langle u\,|\,\beta_1\rangle\left\langle\beta_1\left|F(\hat{k}_s,\,\hat{r};a_2)\right|\beta\right\rangle\right.\\ &\quad \left\langle\beta\left|F(\hat{r},\,\hat{k}_i;a_1)\right|\beta_2\right\rangle\langle\beta_2\,|\,\boldsymbol{\psi_0}\rangle\,\}\\ &\quad \{i(K^*_{zs\alpha_1}-K_{zs\beta_1}+K_{zi\beta_2}-K^*_{zi\alpha_2})\}^{-1}\int_0^d d\zeta\\ &\quad e^{-(\kappa"_{zi\alpha_2}+\kappa"_{zi\beta_2})\zeta}e^{-(k"_\beta+k"_\gamma)\zeta\,\sqrt{1+\eta^2}}\\ &\quad e^{-\zeta^2\eta^2/4\sigma_r^2}e^{i\{(k'_\beta-k'_\gamma)\sqrt{1+\eta^2}-k'_{zi\alpha_2}+k'_{zi\beta_2}\}\zeta}\,]\\ &- \int_0^{2\pi}d\varphi\,Re\,[\,\{\text{same matrices}\}\\ &\quad \{i(K^*_{zs\alpha_1}-K_{zs\beta_1}+K_{zi\beta_2}-K^*_{zi\alpha_2})\}^{-1}\int_0^d d\zeta\\ &\quad e^{-i(K^*_{zs\alpha_1}-K_{zs\beta_1}+K_{zi\beta_2}-K^*_{zi\alpha_2})d}\,e^{(\kappa"_{zs\alpha_1}+\kappa"_{zs\beta_1})\zeta}\\ &\quad e^{-(k"_\beta+k"_\gamma)\zeta\,\sqrt{\{1+\eta^2}}e^{-\zeta^2\eta^2/4\sigma_r^2}\\ &\quad e^{i\{(k'_\beta-k'_\gamma)\sqrt{1+\eta^2}+k'_{zs\alpha_1}-k'_{zs\beta_1}\}\zeta}\,]\\ &+ \int_0^{2\pi}d\varphi\,Re\,[\,\{\text{same matrices with }\widehat{r}\leftrightarrow-\widehat{r}\}\\ &\quad \{i(K^*_{zs\alpha_1}-K_{zs\beta_1}+K_{zi\beta_2}-K^*_{zi\alpha_2})\}^{-1}\int_0^d d\zeta\end{aligned}$$

$$
\begin{aligned}
& e^{-(\kappa"_{zs\alpha_1}+\kappa"_{zs\beta_1})\zeta} e^{-(k"_\beta+k"_\gamma)\zeta\sqrt{1+\eta^2}} \\
& e^{-\zeta^2\eta^2/4\sigma_r^2} e^{i\{(k'_\beta-k'_\gamma)\sqrt{1+\eta^2}-k'_{zs\alpha_1}+k'_{zs\beta_1}\}\zeta} \,] \\
+ & \int_0^{2\pi} d\varphi \, Re\,[\, \{\text{same matrices with } \widehat{r} \leftrightarrow -\widehat{r}\} \\
& \{i(K^*_{zs\alpha_1} - K_{zs\beta_1} + K_{zi\beta_2} - K^*_{zi\alpha_2}\,)\}^{-1} \int_0^d d\zeta \\
& -i(K^*_{zs\alpha_1}-K_{zs\beta_1}+K_{zi\beta_2}-K^*_{zi\alpha_2})d \; e^{(\kappa"_{zi\beta_2}+\kappa"_{zi\alpha_2})\zeta} \\
& e^{-(k"_\beta+k"_\gamma)\zeta\sqrt{1+\eta^2}} \\
& e^{-\zeta^2\eta^2/4\sigma_r^2} e^{i\{(k'_\beta-k'_\gamma)\sqrt{1+\eta^2}-k'_{zi\beta_2}+k'_{zi\alpha_2}\}\zeta} \,] \qquad (14)
\end{aligned}
$$

In Eq. 14, $\zeta = tan\theta$ has been used. Here θ and φ are the polar coordinates of the directional unit vector $\widehat{r}$ defined in the laboratory frame. On performing the integrals, the polar coordinates θ and φ must be converted to the corresponding polar coordinates Θ and Φ in the body frame of spheroids, respectively.

The second order cross term can be represented:

$$
\begin{aligned}
I_C^{(2)} \;=\; & B \int da_1 N(a_1) \int da_2 N(a_2) \{\, 2 \cdot \int_0^\infty d\eta \frac{\eta}{1+\eta^2} \\
& \int_0^{2\pi} d\varphi \, Re\,[\, \Big\{ \langle u \mid \alpha_1 \rangle \Big\langle \alpha_1 \Big| F(\hat{k}_s,\, -\hat{r};\, a_1) \Big| \gamma \Big\rangle \\
& \Big\langle \gamma \Big| F(-\hat{r},\, \hat{k}_i;\, a_2) \Big| \alpha_2 \Big\rangle \langle \alpha_2 \mid \boldsymbol{\psi_0} \rangle \,\}^* \\
& \Big\{ \langle u \mid \beta_1 \rangle \Big\langle \beta_1 \Big| F(\hat{k}_s,\, \hat{r};\, a_2) \Big| \beta \Big\rangle \\
& \Big\langle \beta \Big| F(\hat{r},\, \hat{k}_i;\, a_1) \Big| \beta_2 \Big\rangle \langle \beta_2 \mid \boldsymbol{\psi_0} \rangle \,\} \\
& \{i(K^*_{zs\alpha_1} - K_{zs\beta_1} + K_{zi\beta_2} - K^*_{zi\alpha_2}\,)\}^{-1} \int_0^d d\zeta \\
& e^{-(\kappa"_{zi\beta_2}+\kappa"_{zs\alpha_1})\zeta} e^{-(k"_\beta+k"_\gamma)\zeta\sqrt{1+\eta^2}} e^{-\zeta^2\eta^2/4\sigma_r^2} \\
& e^{i\{(k'_\beta-k'_\gamma)\sqrt{1+\eta^2}-k'_{zs\alpha_1}+k'_{zi\beta_2}-q_{\beta_2\alpha_2\beta_1\alpha_1}\}\zeta} \,] \\
- \; & \int_0^{2\pi} d\varphi \, Re\,[\, \{\text{same matrices}\}\{i(K^*_{zs\alpha_1} - K_{zs\beta_1} \\
& +K_{zi\beta_2} - K^*_{zi\alpha_2}\,)\}^{-1} \int_0^d d\zeta \, e^{-\zeta^2\eta^2/4\sigma_r^2} \\
& e^{-i(K^*_{zs\alpha_1}-K_{zs\beta_1}+K_{zi\beta_2}-K^*_{zi\alpha_2})d} \; e^{(\kappa"_{zs\beta_1}+\kappa"_{zi\alpha_2})\zeta} \\
& e^{i\{(k'_\beta-k'_\gamma)\sqrt{1+\eta^2}-k'_{zs\beta_1}+k'_{zi\alpha_2}-q_{\beta_2\alpha_2\beta_1\alpha_1}\}\zeta} \,] \qquad (15)
\end{aligned}
$$

in which $q_{\beta_2\alpha_2\beta_1\alpha_1}$ denotes the deviation from the right backscattering:

$$
\begin{aligned}
q_{\beta_2\alpha_2\beta_1\alpha_1} \;=\; & 2^{-1}(k'_{i\beta_2} + k'_{i\alpha_2}) sin\theta_{inc} cos(\varphi_{inc} - \varphi) \\
+ \; & 2^{-1}(k'_{s\beta_1} + k'_{s\alpha_1}) sin\theta_s cos(\varphi_s - \varphi) \qquad (16)
\end{aligned}
$$

When the incident angle θ_{inc} is set at π, the backscattering angle becomes 0. As the scattering angle θ_s deviates from the right backscattering angle $\theta_s = 0$, the value of $q_{\beta_2\alpha_2\beta_1\alpha_1}$ increases, resulting in strong decorrelation of the cross term (15). Note that Eqs. 14 and 15 include the effect of spatial anisotropy caused by spheroidal particles. It is also noted that high symmetries of scattering amplitude matrices shown in [8], [9] break out due to introduction of a generic dropsize distribution instead of mono disperse dropsize distribution.

III. Discussion and Conclusion

The main purpose of this paper is to calculate the effects of second order scatterings on the received signal from rains with a generic drop size distribution, such as the Marshall-Palmer distribution. Rain drop shapes can be approximated as spheroids, and a numeric relation between the axial ratio (vertical radius/ horizontal radius = a/b) and the equivolumetric radius a_0(mm) is reported in [12] as

$$
a/b = 1 - 0.1a_0 \qquad (17)
$$

As a first step, the principal axes of spheroids are assumed to be aligned in the vertical direction. Since the second scattering effect appears maximally for the infinite footprint radius [8], [9], Eqs. 14 and 15 are calculated for $\sigma_r = \infty$. The other parameters are matched to those of the CloudSat mission. The layer thickness is taken equal to the vertical resolution of 500 m, and the radar frequency is set at f = 95 GHz. Figure 2 is the result for the Marshall-Palmer distribution with the rain drop shapes defined by Eq. 17. In the figure, the second order ladder terms normalized by the first order scattering (Eq. 12) are denoted as L_2^{co} and L_2^{cx} for the copolarized and cross polarized signals respectively, while the corresponding second order cross terms are denoted as C_2^{co} and C_2^{cx}. Figures 2 (a) and (b) show the copolarized and cross polarized returns respectively. It is noticed that there is no first order contribution to the cross polarization for nadir operation. The formalism of this paper can be applied to only CW radars in rigorous sense. However, for over 5 mm/hr rains along with a large resolution length of 500 m, we can show that this formalism can be used as a first estimator for second order scattering. Figure 2 (a) indicates that the total increment in copolarized return ($1 + L_2^{co} + C_2^{co}$) reaches as high as 2 dB for 10 mm/hr rain. This increment must be subtracted from measured copolarized intensity in order to retrieve the correct amount of precipitation.

The second purpose of this paper is to evaluate the differences in reflectivities up to the second order scattering between spherical and spheroidal shapes. When the principal axes of spheroids are aligned in the vertical direction, there is no spatial anisotropy in the vertical direction so that there is no difference in value of the first order scattering (Eq. 12) between the two rain shapes. However, for the second scattering process, the propagation from one particle to another, especially in the transverse direction, is affected by the anisotropy brought by spheroidal shapes. This effect is considered to be larger in the cross polarization ($L_2^{cx} + C_2^{cx}$) than in the copolarization ($L_2^{co} + C_2^{co}$), because the former has more contribution of transverse propagation. In fact it is found that the values of $L_2^{cx} + C_2^{cx}$ and $L_2^{co} + C_2^{co}$ for the spheres have higher values than those for the spheroids by (< 0.4 dB) and (< 0.1 dB) respectively.

To apply the theory in this paper to pulsed radars, it is necessary to combine it to the time-dependent theory [1], which does not include the effects of the cross term (Eq. 15) nor finite footprint size. The small differences in values of the second order scattering between spheres and spheroids

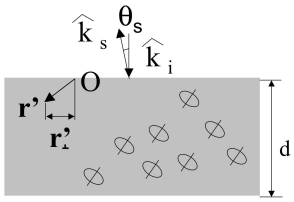

Fig. 1. Schematic diagram of distribution of spheroidal hydrometeors, and the incident $\hat{k}_i$ and the scattered $\hat{k}_s$ wave directions. An arbitrary point in the medium of thickness of d is denoted by $\mathbf{r}'$ The point O is the origin of coordinates in the laboratory frame. The principal axes of spheroids are tilted to the laboratory frame.

indicates that the combined algorithm may be achieved by approximating raindrops as spheres.

ACKNOWLEDGMENT

The research described in this paper was carried out at the Jet Propulsion Laboratory, California Institute of Technology, under a contract with the National Aeronautics and Space Administration.

REFERENCES

[1] Ito, S., T. Oguchi, T. Iguchi, H. Kumagai, and R. Meneghini (1995), Depolarization of radar signals due to multiple scattering in rain, *IEEE Trans. Geosci. and Remote sensing*, vol. 33, pp. 1057-1062.

[2] Iguchi, T., R. Meneghini, and H. Kumagai (1992), Radar depolarization signatures of rains in cumulus clouds measured with dual-frequency airborne radar, *Proc. IGARSS'92 Symp.*, pp. 1728-1730.

[3] de Wolf, D. A. (1971), Electromagnetic reflection from an extended turbulent medium: Cumulative forward scatter single-backscatter approximation, *IEEE Trans. Antenna and Propag.*, Ap-19, pp. 254-262.

[4] Golubentsev, A.A. (1984), Suppression of interference effects in multiple scattering of light, *Soviet Phys. JETP*, vol. 59, pp. 26-32.

[5] Kuga, Y., and A. Ishimaru (1984), Retroflectance from a dense distribution of spherical particles, *J. Opt. Soc. Am.*, A, 1, pp. 831-835.

[6] Mandt, C. E., L. Tsang, and A. Ishimaru (1989), Copolarized and depolarized backscattering enhancement of random discrete scatterers of large size based on second-order ladder and cyclical theory, *J. Opt. Soc. Am.*, A., 7, pp. 585-592.

[7] Tsang, L. and A. Ishimaru (1985), Theory of backscattering enhancement of random discrete isotropic scatterers based on the summation of all ladder and cyclical terms, *J. Opt. Soc. Am.*, A., 2, pp. 1331-1338.

[8] Kobayashi, S., S. Tanelli and E. Im, (2004), Effects of multiple scattering for millimeter-wavelength weather radars, to be published in *International Radiation Symposium (IRS2004)*, Busan, Korea, August 2004.

[9] Kobayashi, S., S. Tanelli, and E. Im, (2004), Backscattering enhancement with a finite beam width for millimeter-wavelength weather radars, *Proc. SPIE, Microwave Remote Sensing. Atmos. Environment IV*, vol. 5654, pp. 106-113.

[10] Bringi, V.N., and V. Chandrasekar (2001), *Polarimetric Doppler weather radar*, Cambridge Univ. Press, Cambridge, UK.

[11] Oguchi, T. (1973), Attenuation and phase rotation of radio waves due to rain: Calculations at 19.3 and 34.8 GHz, *Radio Science*, vol.8, pp. 31-38.

[12] Oguchi, T., (1983), Electromagnetic wave propagation and scattering in rain and other hydrometeors, *Proc. IEEE*, vol. 71, pp. 1029-1078.

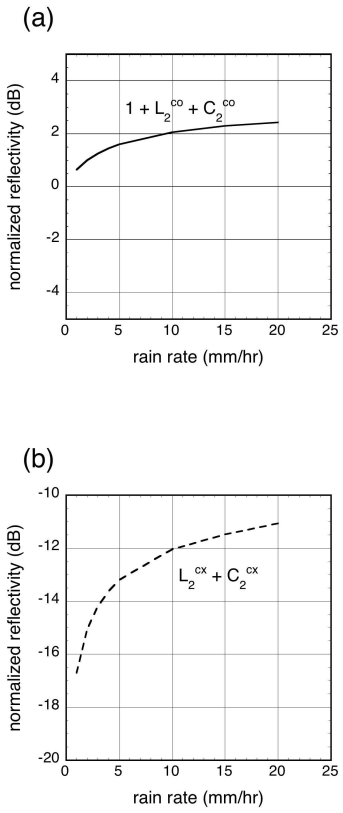

Fig. 2. Increments in total reflectivities as functions of rain rate (mm/hr) for Marshall-Palmer distribution with drop shapes given by Eq. 17. The principal axes of spheroids are in the vertical direction. Nadir operation with radiation frequency 95 GHz is assumed. A layer thickness d, and the footprint radius are set at 500 m and infinity respectively. (a): Copolarized return signal. (b): Cross polarized return signal. Note that there is no first order contribution to the cross polarization for nadir operation.